Numerical modeling and measurement by pulsed television holography of ultrasonic displacement maps in plates with through-thickness defects

J. Carlos López-Vázquez
X. Luís Deán-Ben
Cristina Trillo
Ángel F. Doval
José L. Fernández
Universidade de Vigo
Departamento de Física Aplicada
E. T. S. de Enxeñeiros Industriais
Campus Universitario
36310, Vigo, Spain
E-mail: jclopez@uvigo.es

Faisal Amlani
Oscar P. Bruno
California Institute of Technology
Applied and Computational Mathematics
MC 217-50
Pasadena, California 91125

Abstract. We present a novel numerical modeling of ultrasonic Lamb and Rayleigh wave propagation and scattering by through-thickness defects like holes and slots in homogeneous plates, and its experimental verification in both near and far field by a self-developed pulsed TV holography system. In contrast to rigorous vectorial formulation of elasticity theory, our model is based on the 2-D scalar wave equation over the plate surface, with specific boundary conditions in the defects and plate edges. The experimental data include complex amplitude maps of the out-of-plane displacements of the plate surface, obtained by a two-step spatiotemporal Fourier transform method. We find a fair match between the numerical and experimental results, which allows for quantitative characterization of the defects. [DOI: 10.1117/1.3484953]

Subject terms: pulsed television holography; nondestructive testing; ultrasonics; elastic waves; plates.

Paper 100096PR received Feb. 4, 2010; revised manuscript received Jun. 21, 2010; accepted for publication Jul. 13, 2010; published online Sep. 30, 2010.

1 Introduction

Ultrasonics is one of the classical and most powerful technologies for nondestructive testing (NDT) and evaluation of plate-like structures in industry.[1] In the last few decades, due to simultaneous advances in theoretical studies of elastic wave propagation and scattering, and developments of numerical techniques for obtaining approximate solutions, assessment results of ultrasonics NDT have been progressively more quantitative in an increasing number of applications.[2] Currently, ultrasonics hold a privileged position as a high performance NDT branch and are becoming increasingly competitive, incorporating the newest transducer technologies and information processing schemes. One of the most relevant emergent technologies is optical probing of ultrasound[3] that adds to the well-known classical benefits of ultrasonic techniques (deep-penetration capability with a high degree of interaction with flaws or inhomogeneities, wide temporal bandwidth, high information content, etc.), new potentials typically associated with optical techniques (remote operation capability avoiding contact- or fluid-coupling, high lateral spatial resolution, or the possibility to perform inspections in very small or inaccessible areas).[4]

In our case, we have demonstrated that the nondestructive inspection of plates can be performed by using 2-D acoustic fields of instantaneous out-of-plane displacements obtained with a self-developed pulsed TV holography system.[4,5] The ultrasonic 2-D field maps the elastic wave scattering patterns that contain information related to defects (position, dimensions, orientation, etc.). For obtaining a quantitative characterization on this basis, the most direct and reliable possibility would be to adapt to our system output one of the existing numerical schemes based on the vectorial linear theory of elasticity (Refs. 6–11). Nevertheless, selection among this wide spectrum of possible models (and its subsequent adaptation) is far from being direct in our case, and the main reasons are two-fold. On the one hand, in contrast to more classical ultrasonic schemes (pulse-echo or pitch-catch classical configurations) that provide outputs with high temporal resolution and low spatial information content, our system presents complementary characteristics providing information with high spatial resolution, i.e., a large number of spatial samples (about 10^6) at a much smaller number of temporal samples (typically eight). On the other hand, the field of view of the detected 2-D scattering pattern includes both near- and far-field zones and includes tens of ultrasonic wavelengths, which means that the modeling of the wave propagation and interaction has to be adequate within the mid-high frequency range. These two features invalidate or limit the applicability of many existing approaches that have been designed for high temporal resolution outputs and/or low frequency regime.

An alternative to vectorial models is to employ simplified theories as the basis for numerical or analytical approximations. These types of models that are valid only for a limited number of situations but that occur often in practice could have wide applicability. In particular, plate theories have been employed for analyzing the scattering of guided waves by cylindrical inclusions in plates[12,13] showing good agreement in the near field when compared with experimental 2-D ultrasonic field distributions detected

0091-3286/2010/$25.00

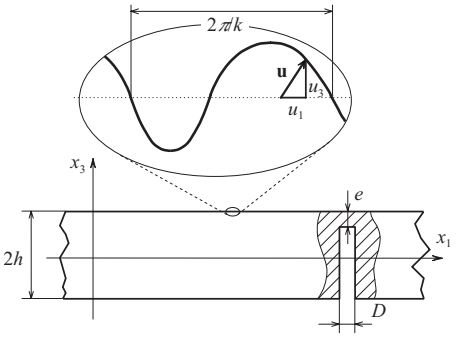

Fig. 1 Scheme of a plate of thickness $2h$ with a cylindrical defect of diameter D and residual depth e. As an example, a detail of the instantaneous surface displacement associated to an harmonic guided wave that propagates along axis x_1 with wavenumber k is shown.

with scanning optical heterodyne interferometry[14] or shearography.[15] Also, a 2-D scalar model has been employed for solving the inverse problem of scattering by cylindrical inclusions in plates using experimental data obtained with a whole-field TV-holography technique close to ours.[16] Reported results in Ref. 16 also include the presentation of near- and far-field simulated scattering patterns for different defect types, but a direct comparison between simulated and experimental ultrasonic field values is not presented.

In this work we present a novel numerical modeling of ultrasonic Lamb and Rayleigh wave propagation and scattering by through-thickness defects in homogeneous plates, and its verification by comparison with experimental complex amplitude maps of the out-of-plane displacements of the plate surface obtained by a self-developed pulsed TV holography system combined with a two-step spatiotemporal Fourier transform method. We introduce the theoretical framework for modeling in the harmonic regime, and outline the state of the art numerical method employed for obtaining simulated scattering data. The procedure for obtaining experimental data by TV holography, combined with the two-step spatiotemporal Fourier transform method that has been described in detail in previous works (see Refs. 4, 5, 17, and 18), is only briefly outlined here, including essential points for completeness. Comparison between experimental and simulated scattering patterns of narrowband guided waves with holes and slots in aluminum plates shows a fair match, both in near- and far-field zones, which allows a subsequent quantitative characterization of the defects on this basis. To the best of our knowledge, apart from our corresponding recent presentation in a congress,[19] this is the first time that such a comparison is reported.

2 Theoretical Framework

2.1 *Linear Elasticity Theory*

The basic relations of linear elasticity theory[20] are included here to establish notation and the framework of the simplified scalar model presented later in Sec. 2.3. Referring to the geometry of Fig. 1, (x_1,x_2,x_3) denote cartesian coordinates, $\mathbf{u}=(u_1,u_2,u_3)$ the displacement vector, and

$$\epsilon_{ij}=\frac{1}{2}\left(\frac{\partial u_i}{\partial x_j}+\frac{\partial u_j}{\partial x_i}\right), \tag{1}$$

are the components of the strain tensor $\boldsymbol{\epsilon}$ for the small (infinitesimal) strain regime. In the case of a linear isotropic solid, its material characteristics can be specified only by Lamé constants λ_L and μ_L, and the stress-strain relationship simplifies to

$$\tau_{ij}=\lambda_L\delta_{ij}\sum_k \epsilon_{kk}+2\mu_L\epsilon_{ij}, \tag{2}$$

with τ_{ij} being the stress tensor components and δ_{ij} the Kronecker delta. In the following we restrict ourselves to harmonic time dependence in such a way that for a single temporal frequency f we have

$$\mathbf{u}(\mathbf{r},t)=\mathrm{Re}[\hat{\mathbf{u}}(\mathbf{r},t)]=\mathrm{Re}[\hat{\mathbf{u}}_m(\mathbf{r})\exp(j2\pi ft)], \tag{3}$$

with $\hat{\mathbf{u}}$ being the complex displacement, $\hat{\mathbf{u}}_m$ the complex amplitude vector of the wave, and j the imaginary unit. In these conditions, employing Eqs. (1) and (2) in a balance momentum equation for a region free of body forces results in

$$(\lambda_L+\mu_L)\,\nabla(\nabla\cdot\hat{\mathbf{u}}_\mathbf{m})+\mu_L\nabla^2\hat{\mathbf{u}}_\mathbf{m}+\rho\omega^2\hat{\mathbf{u}}_\mathbf{m}=0, \tag{4}$$

where ρ is the mass density and $\omega=2\pi f$ is the circular frequency. Equation (4) is the well-known Lamé-Navier equation for a harmonic regime. Displacement $\mathbf{u}$ associated by Eq. (3) to any complex amplitude $\hat{\mathbf{u}}_\mathbf{m}$ that is the solution of this equation can be discomposed in longitudinal $\mathbf{u}_L$ and transversal $\mathbf{u}_T$ components that propagate respectively with phase velocities

$$c_L=\sqrt{\frac{\lambda_L+2\mu_L}{\rho}}, \tag{5}$$

$$c_T=\sqrt{\frac{\mu_L}{\rho}}. \tag{6}$$

2.2 *Guided Waves in Plates and the Two-Dimensional Helmholtz Scalar Equation*

Wave propagation in plates is usually analyzed in terms of particular combinations (called modes) of longitudinal and transversal displacement, characterized by transversal stationary displacement distributions.[20] For a given temporal frequency, each mode travels along a direction contained in plane (x_1,x_2) with a characteristic phase velocity ω/k, with k being the corresponding wavenumber of the mode. In the most common case of plates with stress-free boundaries, modes can be classified into two groups: the so-called horizontal shear (SH) modes that have displacement vectors $\mathbf{u}_{\mathrm{SH}}$ parallel to plane (x_1,x_2), and the Lamb modes, with displacement vectors $\mathbf{u}_{\mathrm{SV}}$ that have in-plane and out-of-plane components (see Fig. 1) and are characterized by the frequency spectrum represented in Fig. 2.

SH modes can be described in terms of one scalar potential, but Lamb modes are usually described by using scalar and vector potentials simultaneously (see Ref. 20). Recently, an alternative has been developed by Achenbach

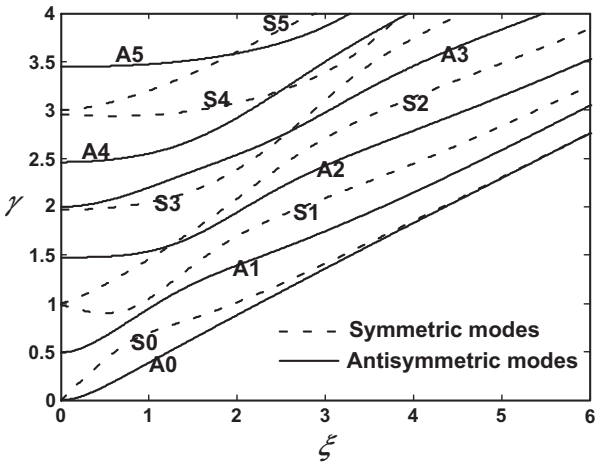

Fig. 2 Frequency spectrum of Lamb modes for a plate with stress-free boundaries. $\gamma=2h\omega/\pi c_L$ and $\xi=2hk/\pi$ are the normalized frequency and wave number, respectively.

that describe Lamb modes with only one scalar potential ϕ and two 1-D functions $W_n(x_3)$ and $V_n(x_3)$ that characterize transversal shapes for the mode labeled n.[21] The out-of-plane component is simply given by $u_{n,3}=W_n(x_3)\phi(x_1,x_2)$. Hence, as the scalar potential $\phi(x_1,x_2)$ verifies the 2-D scalar Helmholtz equation in plane (x_1,x_2), it is evident that for each mode n, the equation

$$\nabla^2\hat{u}_{n,3m}+k_n^2\hat{u}_{n,3m}=0, \tag{7}$$

is also verified for any plane x_3=constant within the plate. In the following, the symbol ∇^2 denotes the 2-D Laplacian operator in (x_1,x_2), and k_n the Lamb wavenumber for mode n.

2.3 *Scattering of Guided Waves in Plates by Through-Thickness Defects*

At this point we restrict the scope of the analysis to scattering phenomena generated by defects with 2-D geometry (as the case of a through-thickness hole with residual depth $e=0$, see Fig. 1). In these conditions, plate geometry is 2-D, in the sense that it depends only on (x_1,x_2) coordinates. When scattering is produced in conditions in which only one propagating Lamb mode contributes to u_3, then Eq. (7) can be employed. Following the approach of Ref. 16, we assume that this is the case.

Then, if Γ denotes the boundary of the 2-D through-thickness defect and $\hat{u}_{3m}$ denotes a complex amplitude associated to the out-of-plane component $u_3(x_1,x_2,h)$ of the scattered field, we can model our problem by means of the partial differential equation,

$$\begin{cases} \nabla^2\hat{u}_{3m}+k^2\hat{u}_{3m}=0 \text{ outside } \Gamma \\ \left.\dfrac{\partial\hat{u}_{3m}}{\partial n}\right|_{\Gamma}=g, \end{cases}, \tag{8}$$

where g is a function defined on Γ. Stress-free conditions at defect boundaries imply conditions on the spatial derivatives of the scattered field as a function of the spatial derivatives of the incident field. For this reason, a generic Neumann boundary condition is stated.

The validity of this model can be justified *a posteriori* on the basis of the comparison of model results with experimental data. Nevertheless, and although it is not the objective of this work to justify the model in Eq. (8) and its conditions of applicability from fundamental equations of linear elasticity in Eqs. (1)–(4), we provide a brief *a priori* justification of our assumption for the case of through-thickness defects. This can be done by referring to an analytical model based on the Achenbach approach for describing the scattering of Lamb waves by cylindrical holes in plates.[22] In particular, it follows from the theoretical discussion presented in this reference that an exact description of the scattering processes under consideration requires adequate account of mode conversion and appearance of SH and Lamb evanescent modes, which result from the stress-free boundary conditions and associated interactions of the incoming waves with the cylinder boundary. Nevertheless, for defects with 2-D geometry, modal conversion occurs only between in-plane components. This means that u_3 displacements for Lamb modes are not mixed with contributions of SH modes. Also, a few wavelengths away from the defect, contributions of the evanescent modes are not relevant. Provided the evanescent modes are also small in the neighborhood of the cylinder boundary, the out-of-plane component can be described everywhere as a superposition of incident and scattered Lamb modes. When only one propagating Lamb mode contributes to the out-of-plane component, the Helmholtz equation is completely justified. When several Lamb-mode contributions exist of a given (fixed) frequency, the same can be stated as far as the corresponding Lamb wave numbers are nearly coincident. This is the case of Rayleigh waves that can be understood in the context of guided waves in plates as a superposition of S0 and A0 modes in their overlapping zone of the spectrum (see Fig. 2).

3 Materials and Methods

3.1 *Test Plates*

Experiments were performed in aluminium plates with dimensions $300\times100\times10$ mm^3 and with through-thickness holes and slots adequately prepared. The longitudinal wave velocity was measured by means of the classical pulse-echo method, resulting in $c_L=6358$ m/s.

Areas without defects were employed for analyzing the incident field. Boundary conditions were studied employing the edge of the plates. In all cases, plates were supported so that the constraints at their surfaces are minimized; they simply rest on a horizontal board covered in velvet fabric. Plasticine was used as an acoustic absorber at the edges of the plates to avoid reflections of the incident and scattered waves that could disturb the measured acoustic fields (Fig. 3).

3.2 *Experimental Setup and Procedure for Obtaining the Experimental Complex Amplitude*

The layout of the experimental system used to generate and detect the elastic waves is depicted in Fig. 4.

Rayleigh waves were generated by means of the classical wedge method, in which the longitudinal wave emitted

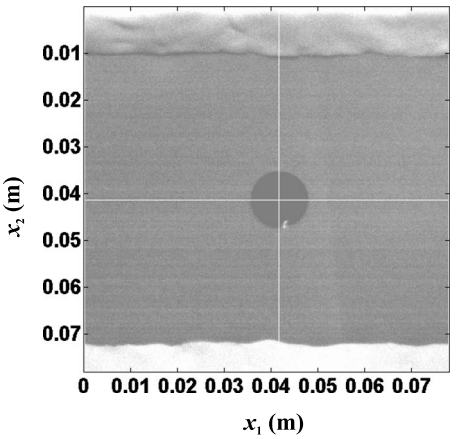

Fig. 3 Reference image for a through-thickness hole ($e=0$) of diameter $D=12$ mm.

by a piezoelectric transducer is coupled to the plate surface through a Bakelite prismatic coupling block (wedge) of angle $\theta_w=65$ deg (Fig. 4). A long tone burst consisting of 99 cycles with a central frequency $f=1.000$ MHz was used to excite the piezoelectric in a way that the generated Rayleigh wave trains are quasimonochromatic. Under these circumstances, the stress at the plate surface caused by the wedge presents a spatial period and has a phase velocity that correspond, respectively, to wavelength λ_R and phase velocity c_R of the Rayleigh wave at frequency f. The wavelength of the produced quasimonochromatic Rayleigh wave λ_R was measured with the procedure described in Ref. 23, resulting in $\lambda_R=2.96$ mm, so that the Rayleigh phase velocity is given by $c_R=\lambda_R f$, resulting in $c_R=2960$ m/s.

On the other hand, the instantaneous out-of-plane acoustic field $u_3(\mathbf{r},t)$ at the plate surface due to the propagation of the Rayleigh wave train is measured with a self-developed double-pulsed TV holography system,[5] which has been successfully employed to measure quasimonochromatic guided waves in plates with nonspecular finish (a discussion of the advantages of TV holography compared to other whole-field and pointwise techniques to probe ultrasound can be found in Ref. 4). As is common in TV

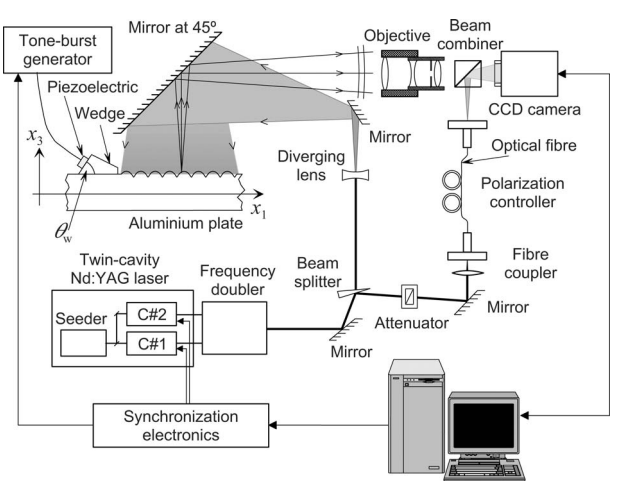

Fig. 4 Experimental setup.

holography techniques,[24] we employ a configuration of an image hologram, sensitive to the out-of-plane component of the displacement of the surface points, with the image sensor of a video camera as a recording medium. There is no optical reconstruction of the recorded holograms, but instead their intensity distribution is electronically processed to render the optical phase-difference map, which depends on the displacements of the specimen surface. The core of the TV holography system is a twin-cavity pulsed, injection-seeded, and frequency-doubled Nd:YAG laser (Spectron SL404T) that emits two laser pulses with a duration of 20 ns and a controlled relative temporal delay. The two pulses are employed for obtaining two correlograms that are recorded successively in separate frames of a charge-coupled device (CCD) camera [(PCO Kelheim, Germany) Sensicam Double-Shutter]. Each correlogram corresponds to the interference of the reference beam and the object beam scattered back by the plate surface.

A processing procedure based on the spatial Fourier transform method is applied to the correlograms,[17] which renders the so-called optical phase-change map $\Delta\Phi(\mathbf{r},t)$, proportional to the instantaneous out-of-plane acoustic displacement field $u_3(\mathbf{r},t)$, i.e.,

$$\Delta\Phi(\mathbf{r},t)=\frac{8\pi}{\lambda}u_3(\mathbf{r},t), \tag{9}$$

with $\lambda=532$ nm being the wavelength of the laser and t the instant of emission of the first laser pulse. The usual scaling factor $(4\pi/\lambda)$ between the optical phase change and displacement is doubled in Eq. (9) by selecting a delay between laser pulses (i.e., between the two correlograms) equal to an odd number of half-periods of the detected Rayleigh wave. For the case of the experiments presented in this study, we have employed a delay of three half-periods (that is the minimum number of odd half-periods for which the camera can record the two correlograms in different frames).

The optical phase-change map given by Eq. (9) represents itself as a useful means to assess the interaction of the Rayleigh wave and defect. However, a second processing procedure based on the Fourier transform can be applied to improve signal-to-noise ratio and calculate the acoustic amplitude $u_{3m}(\mathbf{r})=\mathrm{mod}[\hat{u}_3(\mathbf{r},t)]$ and the total acoustic phase $\varphi_{3T}(\mathbf{r},t)=\arg[\hat{u}_3(\mathbf{r},t)]$ of the Rayleigh wave, from which the complex amplitude

$$\hat{u}_{3m}(\mathbf{r})=u_{3m}(\mathbf{r})\exp[\varphi_m(\mathbf{r})], \tag{10}$$

of the ultrasonic field can be obtained by simply selecting an arbitrary value of time t_0, for which $\varphi_m(\mathbf{r})=\varphi_{3T}(\mathbf{r},t_0)$. Our procedure,[18] which consists of an improved version of a previous method described in Ref. 17, is based on the spatiotemporal 3-D Fourier transform of a set of optical phase-change maps corresponding to successive instants delayed by a quarter of the wave period. As long as the ultrasonic waves are narrowband, most of the spectral energy is contained in a small region of the spatial frequency plane and within a thin slice of temporal frequencies, and can be easily filtered and inverse Fourier transformed to obtain the mechanical amplitude and phase of the wave. The selection of the number of maps [apart from the fact

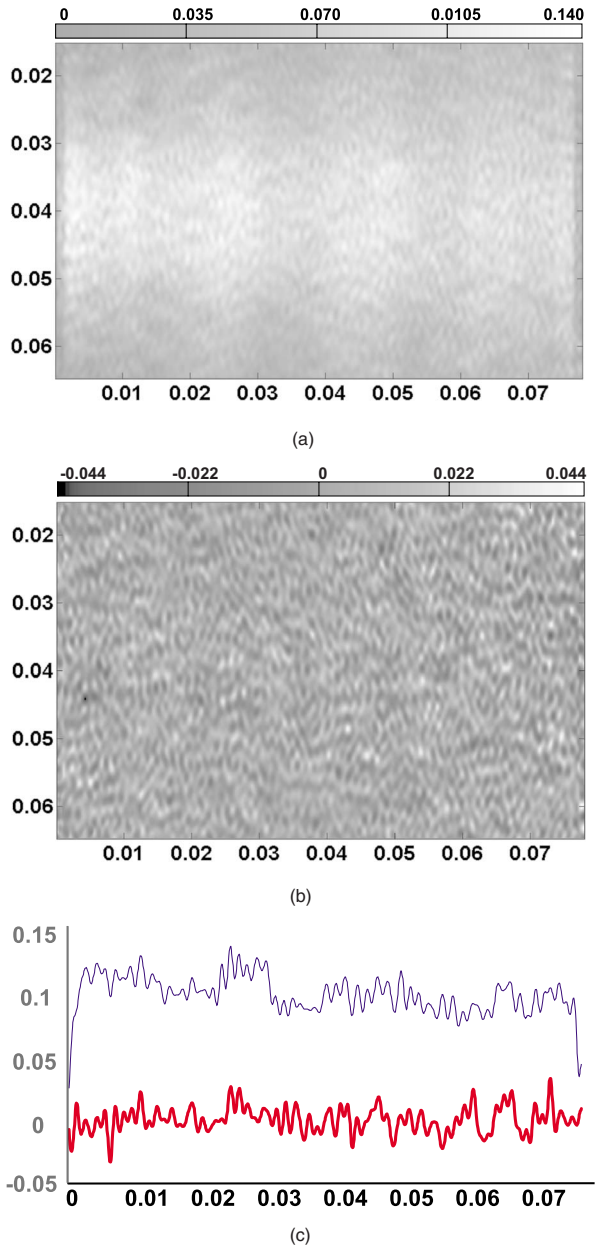

Fig. 5 Repeatability results. (a) Modulus of reference incident field, (b) difference of the modulus of reference field and another equivalent incident field, and (c) horizontal profiles of (a) (thin) and (b) (thick). Dimensions are in meters. Midgray level represents zero. Grayscale bars in (a) and (b) and profile amplitude in (c) are in units of $\lambda/4\pi$. The axis numbering in (a) and (b) corresponds to that of Fig. 3.

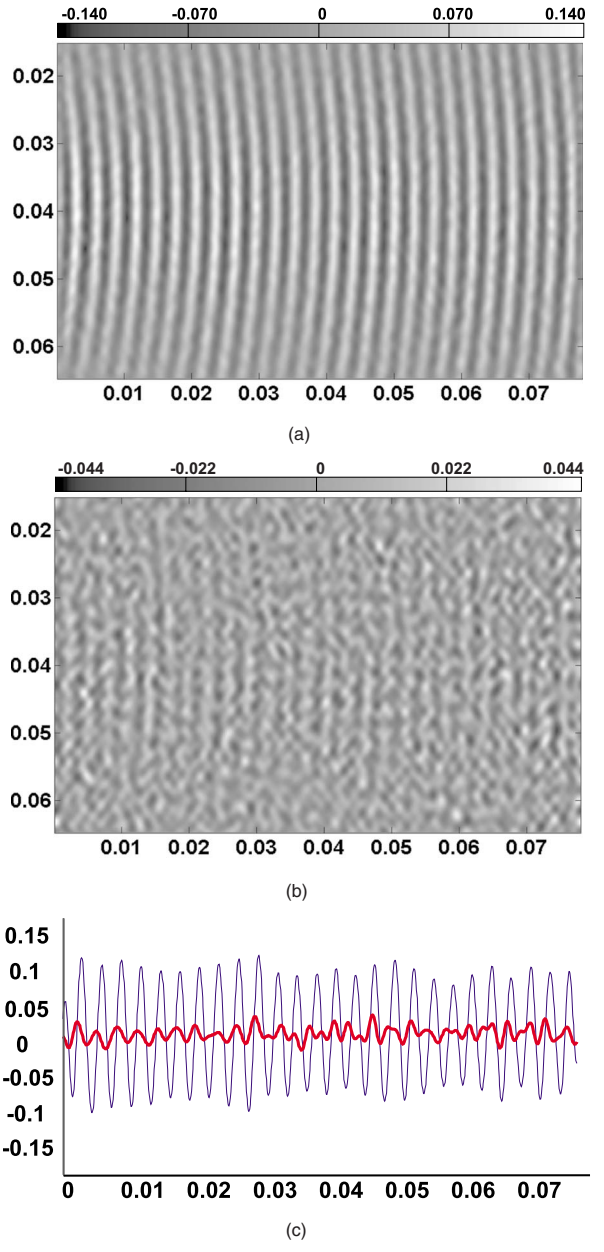

Fig. 6 Repeatability results. (a) Real part of reference incident field, (b) difference of the real parts of reference field and another equivalent incident field, and (c) horizontal profiles of (a) (thin) and (b) (thick). Dimensions are in meters. Midgray level represents zero. Grayscale bars in (a) and (b) and profile amplitude in (c) are in units of $\lambda/4\pi$. The axis numbering in (a) and (b) corresponds to that of Fig. 3.

that it must be an integer power of 2 to employ fast-Fourier transform (FFT) algorithms] stems from a compromise between the attainable improvement of the signal-to-noise ratio of the measured displacements and the data acquisition cost (time and computational resources). In our case, eight optical phase-change maps delayed 250 ns were taken in each experiment, and the spatiotemporal 3-D Fourier transform method was applied to the whole set. The obtained experimental complex amplitude is the raw data for the comparison with numerical simulations.

3.3 *Numerical Method*

To efficiently produce accurate solutions for Eq. (8), we utilize a modified version of a highly efficient and accurate numerical methodology introduced recently,[25] which we describe briefly in what follows.

As is well known, the (unique) solution of the Neumann problem in Eq. (8) can be expressed as a double-layer potential

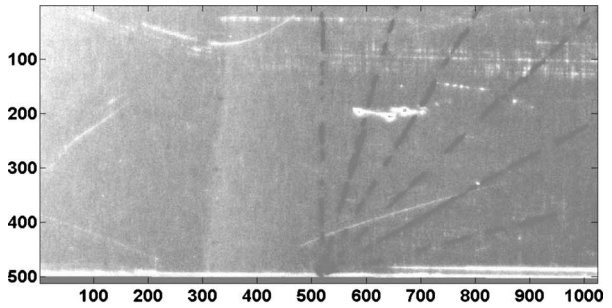

(a)

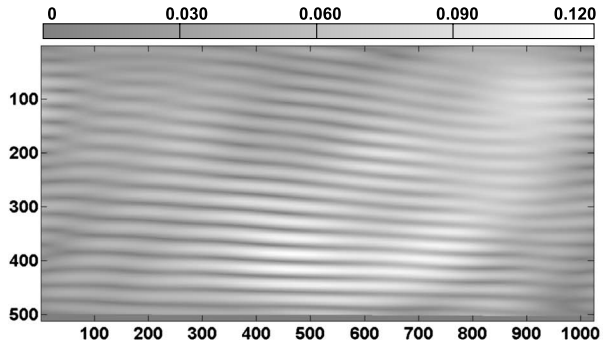

(b)

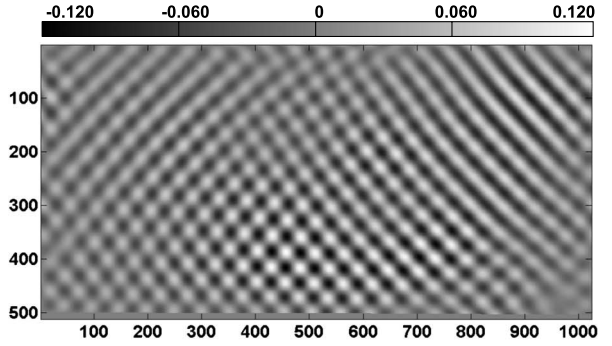

(c)

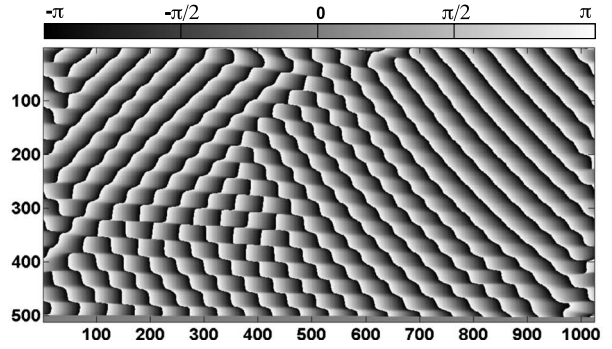

(d)

Fig. 7 Results for the boundary conditions at the edge of the plate for an incident angle of 45 deg. (a) Reference image (in white light) of the plate and the edge, which is the horizontal transition at pixel 500, and (b), (c), and (d) are modulus, real part, and phase of the complex amplitude of the total field, respectively. Dimensions are in pixels. Midgray level represents zero. Grayscale bars in (b) and (c) are in units of $\lambda/4\pi$. The axis numbering of (a), (b), (c), and (d) corresponds to that of Fig. 3. Note that in (b), (c), and (d) the values are zero for pixels located outside the plate area below the edge transition.

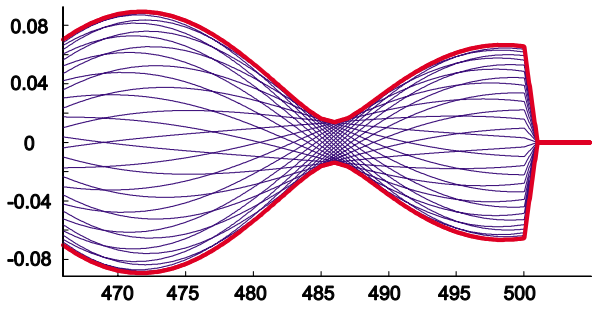

(a)

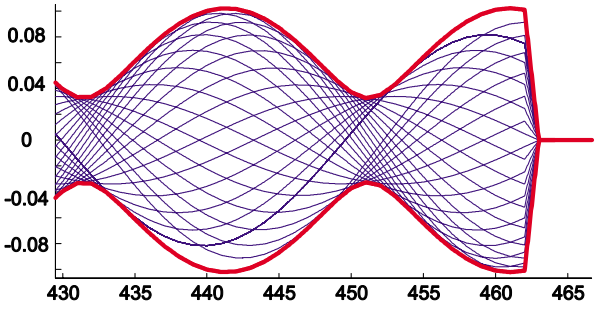

(b)

Fig. 8 Results for the boundary conditions at the edge of the plate. Measured profiles of the real part of the complex amplitude of the total field for several time delays (thin) with the modulus envelope (thick) for incident angle of (a) 45 deg and (b) 0 deg. Dimensions are in pixels. Profile amplitude in units of $\lambda/4\pi$. All profiles include zero displacement values for pixels outside the plate area (see Fig. 7), which generates the artifact of a cone that converges to zero, just after the edge, on the right.

$$\hat{u}_{3m}(\mathbf{r}) = \int_{\Gamma} \frac{\partial G_k(\mathbf{r},\mathbf{r}')}{\partial \mathbf{n}'_{\mathbf{r}}} \mu(\mathbf{r}')d\ell'. \tag{11}$$

Here G_k denotes the Hankel function

$$G_k(\mathbf{r},\mathbf{r}') = \frac{i}{4} H_0^1(k|\mathbf{r}-\mathbf{r}'|), \tag{12}$$

and, letting N denote the hypersingular operator,

$$N(\mu)(\mathbf{r}) = \lim_{z\to\infty} \frac{\partial}{\partial \mathbf{n}_{\mathbf{r}}} \int_{\Gamma} \frac{\partial G_k(\mathbf{r},\mathbf{r}'+z\mathbf{n}_{\mathbf{r}'})}{\partial \mathbf{n}'_{\mathbf{r}}} \mu(\mathbf{r}')d\ell', \tag{13}$$

the density μ is the unique solution of the first kind integral equation

$$N(\mu) = g. \tag{14}$$

Once the unknown surface density μ has been obtained, the solution $\hat{u}_{3m}$ of Eq. (8) can be produced at any point outside Γ by applying numerical quadrature to Eq. (11).

Our numerical solver produces approximate solutions μ of Eq. (14) for a given right-hand side g by seeking a set of values $\mu_j \approx \mu(\mathbf{r}_j)$ of the unknown μ at a set of points $\mathbf{r}_j$ $(j=1,\ldots,n)$ on the curve Γ. The algorithm relies on a highly accurate approximation of the integral in Eq. (14), which can be obtained by appealing to an expression of the right-hand side of Eq. (13) that only uses tangential derivatives, in conjunction with interpolation of the values μ_j by

trigonometric polynomials, and exact differentiation and integration of trigonometric monomials. To resolve high curvatures while taking advantage of the excellent properties of trigonometric interpolation, the method utilizes smooth changes of variables that map an equispaced grid in the interval $[0,2\pi]$ to a grid on Γ that contains a high density of discretization points $\mathbf{r}_j$ in high curvature portions of Γ. Note, in particular, that as a result of this discretization strategy, the density of discretization points $\mathbf{r}_j$ varies smoothly along Γ. The method then proceeds by constructing a linear system of equations for the quantities μ_j, which arises as the discretized version of the left-hand-side in Eq. (14) is set to equal the right-hand side of that equation at each point $\mathbf{r}_j$, $j=1,\ldots,n$. The algorithm is then completed by solving this linear system by means of a numerical implementation of the Gaussian elimination method. It was verified through a variety of numerical experiments, including comparisons with exact solutions, that the solutions $\hat{u}_{3m}$ produced by this methodology are highly accurate, and that the associated errors decay rapidly as discretizations are refined.

4 Results and Discussion

4.1 *Incident Field Characterization*

To know the characteristics of the incident acoustic field and the repeatability of the measured maps, a series of acquisitions in the same conditions was performed at time intervals of 5 min. After processing the raw images in the same manner with identical parameters, the modulus [Fig. 5(a)] and the real part [Fig. 6(a)] of the acoustic field were obtained. The deviations between maps [Figs. 5(b) and 6(b)] were of the order of 20% for both amplitude [Fig. 5(c)] and real part [Fig. 6(c)]. Taking into account that the typical value of the amplitude was about 5 nm, these values are in accordance with a previous estimation of the noise of the technique.[4] Other features of interest are the slight curvature of the wavefronts, clearly noticeable in Fig. 6(a), and a nonuniform amplitude profile in a section transverse to the main propagation direction [visible as the gray-level variation along any vertical line in Fig. 5(a)]. Both features complicate the comparison between experimental and numerical results.

4.2 *Boundary Conditions*

To gain understanding about the boundary conditions to apply at the border of the defects, we studied the reflection of the incident acoustic field at the straight edge of a plate without defects for different incidence angles. The obtained results (Figs. 7 and 8) approximately correspond to the superposition of two plane traveling waves of similar (but not equal) amplitudes, with the reflection angle equal to the incidence one. Although the observed boundary conditions are neither Dirichlet nor Neumann, they are not far from the Neumann ones [i.e., $g=0$ in Eq. (8)]. So, we adopted them as a starting point for the numerical simulations of the scattering patterns.

4.3 *Scattering Patterns*

In Figs. 9 and 10, the comparison between the experimental and simulated scattering patterns of Rayleigh waves corresponding to a hole and a slot are presented. A simple visual

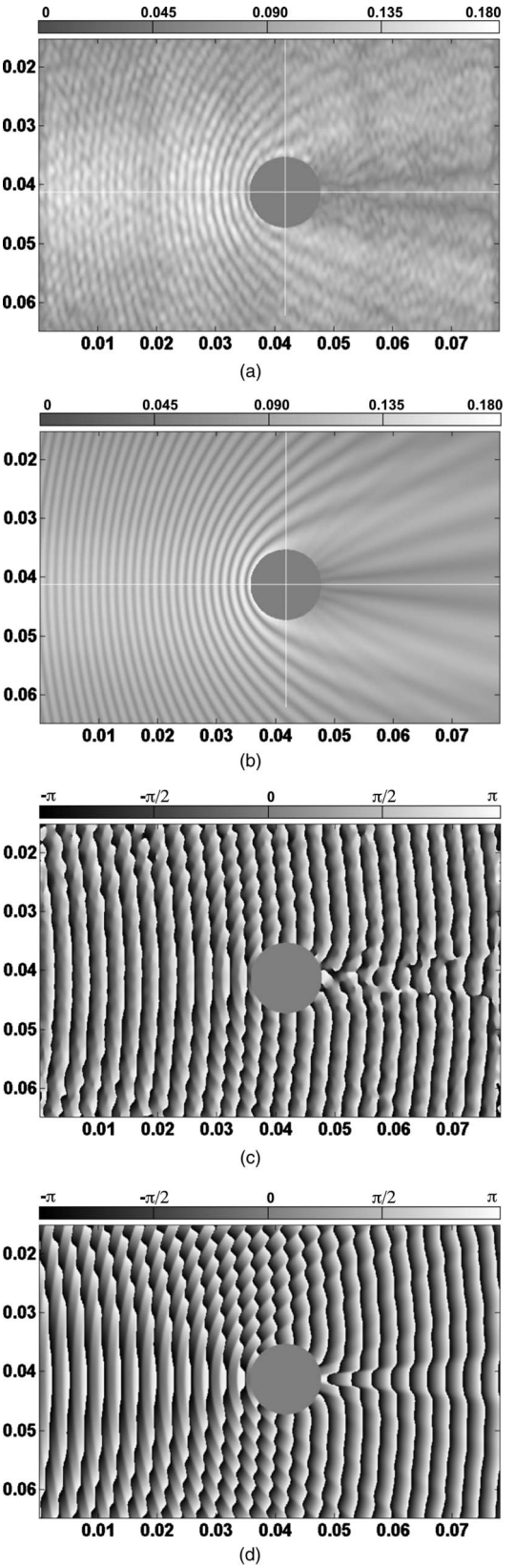

Fig. 9 Scattering patterns for a cylindrical hole with $D=12$ mm. Comparison of complex amplitudes: (a) and (c) are experimental, (b) and (d) are numerical; (a) and (b) are the modulus, and (c) and (d) phase. Dimensions are in meters. Midgray level represents zero. Grayscale bars in (a) and (b) are in units of $\lambda/4\pi$. The axis numbering corresponds to that of Fig. 3.

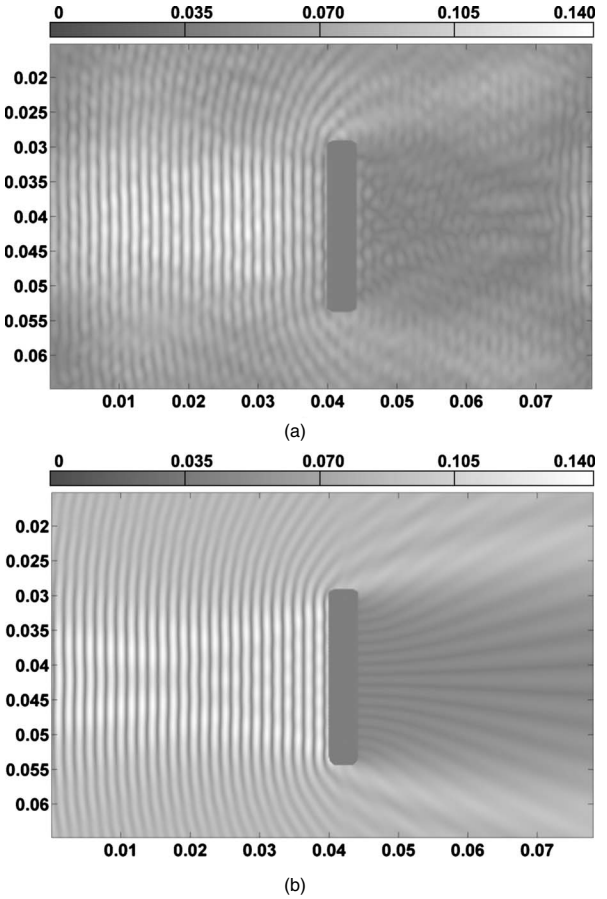

Fig. 10 Scattering patterns for a slot of mean width of 4.4 mm and length of 24 mm. Modulus of complex amplitude: (a) experimental and (b) numerical. Dimensions are in meters. Midgray level represents zero. Grayscale bars in (a) and (b) are in units of $\lambda/4\pi$. The axis numbering corresponds to that of Fig. 3.

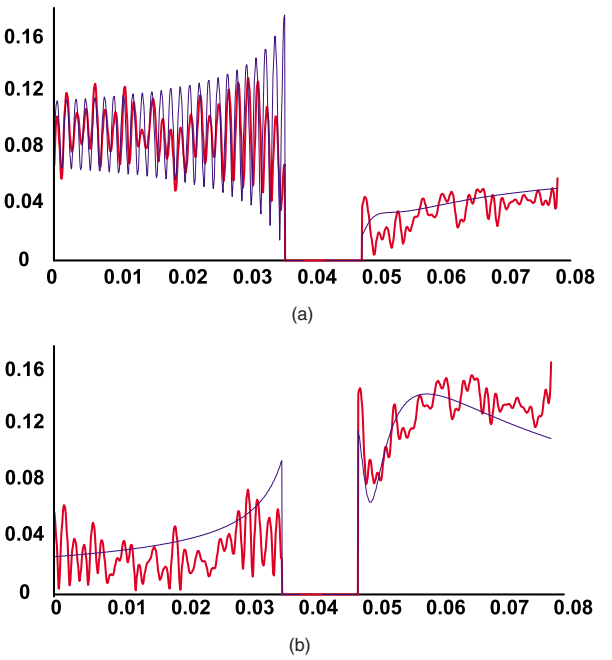

Fig. 11 Profiles along the white horizontal line marked in Fig. 3 correspond to maps of Fig. 9: (a) modulus of complex amplitude of the total field, (b) modulus of complex amplitude of scattered field, (thick) experimental, and (thin) numerical. Profile amplitude is in units of $\lambda/4\pi$.

inspection reveals their close agreement both in modulus and phase. Small differences between Figs. 10(a) and 10(b) can be observed that are most noticeable in the shadow region and could be associated, among other reasons, to the neglect in our 2-D approximation of the near-field evanescent modes. For quantitative comparison, the profiles along a central line of the maps, both for the total and scattered fields, are presented (Fig. 11). Even though the main features of the scattering pattern appear well correlated, the pixel-to-pixel agreement between maps is not as good as their 2-D visual matching. This is in consonance with measured noise levels. At this point, image processing techniques that average or reject noise on the basis of spatial or morphological filtering could be applied. A more comprehensive analysis of these issues will be addressed in future work, but in any case, we believe that the presented results are enough to say that the experimental contrast of the numerical simulation is positive.

5 Conclusions

Scattering of elastic waves in plates is studied, employing 2-D maps of instantaneous out-of-plane displacements obtained with a self-developed pulsed TV holography system. Experimental data are compared with simulated scattering patterns employing a state of the art numerical technique. The achieved agreement gives support to the employed 2-D model. To improve the reliability of this model, further work should be done to analyze more defect typologies and sizes under different Lamb modes and frequencies.

Acknowledgments

This work was cofunded by the Spanish Ministerio de Ciencia e Innovación and by the European Comission (ERDF) in the context of the Plan Nacional de I+D+i (project number DPI2008-02709), and by the Dirección Xeral de Investigación, Desenvolvemento e Innovación da Xunta de Galicia in the context of the Plan Galego de IDIT (project number INCITE08PXIB303252PR). Supplementary cofunding from the Universidade de Vigo (project number I608122F64102) is also acknowledged. Amlani and Bruno gratefully acknowledge support by the Air Force Office of Scientific Research and the National Science Foundation.

References

1. *Nondestructive Testing Handbook*, 2nd ed., vol. **7**, A. S. Birks, R. E. Green Jr., and P. McIntire, Eds., pp. 1–215, Ultrasonic Testing, American Society for Nondestructive Testing, Columbus, OH (1991).
2. L. J. Bond, "Numerical techniques and their use to study wave propagation and scattering—a review," in *Elastic Waves and Ultrasonic Nondestructive Evaluation*, Y. S. Rajapakse, S. K. Datta, and J. D. Achenbach, Eds., pp. 17–27, Elsevier Science Publisher (1990).
3. C. B. Scruby and L. E. Drain, *Laser Ultrasonics. Techniques and Applications*, Adam Hilger, Bristol, United Kingdom (1990).

4. J. L. Fernández, A. F. Doval, C. Trillo, J. L. Deán, and J. C. López, "Video ultrasonics by pulsed TV holography: a new capability for non-destructive testing of shell structures," *Intl. J. Optomechatron.* **1**, 122–153 (2007).
5. C. Trillo, D. Cernadas, A. F. Doval, C. López, B. V. Dorrío, and J. L. Fernández, "Detection of transient surface acoustic waves of nanometric amplitude with double-pulsed TV holography," *Appl. Opt.* **42**, 1228–1235 (2003).
6. Y. Cho and J. L. Rose, "A boundary element solution for a mode conversion study on the edge reflection of lamb waves," *J. Acoust. Soc. Am.* **99**, 2097–2109 (1996).
7. B. Morvan, N. Wilkie-Cahncellier, H. Duflo, A. Tinel, and J. Duclos, "Lamb wave reflection at the free edge of a plate," *J. Acoust. Soc. Am.* **113**, 1417–1425 (2003).
8. M. Castaings, E. Le Clezio, and B. Hosten, "Modal decomposition method for modeling the interaction of lamb waves with cracks," *J. Acoust. Soc. Am.* **112**, 2567–2582 (2002).
9. B. Masserey and E. Mazza, "Analysis of the near-field ultrasonic scattering at a surface crack," *J. Acoust. Soc. Am.* **118**, 3585–3594 (2005).
10. G. R. Liu, "A combined finite element/strip method for analysing elastic wave scattering by cracks and inclusion in laminates," *Comput. Mech.* **28**, 76–81 (2002).
11. S. Banerjee and T. Kundu, "Scattering of ultrasonic waves by internal anomalies in plates," *Opt. Eng.* **46**, 053601-1 to -9 (2007).
12. C. Vemula and A. N. Norris, "Flexural wave propagation and scattering of on thin plates using Mindlin theory," *Wave Motion* **26**, 1–12 (1997).
13. C. H. Wang and F. K. Chang, "Scattering of plate waves by a cylindrical inhomogeneity," *J. Sound Vib.* **282**, 429–451 (2005).
14. P. Fromme and M. B. Sayir, "Measurement of the scattering of a Lamb wave by a through hole in a plate," *J. Acoust. Soc. Am.* **111**, 1165–1170 (2002).
15. F. Taillade, "Association de la shearographie et des ondes de Lamb pour la détection rapide et quantitative des délaminages," PhD Thesis, Conservatoire National des Arts et Métiers (2000).
16. T. D. Mast and G. A. Gordon, "Quantitative flaw reconstruction from ultrasonic surface wavefields measured by electronic speckle pattern interferometry," *IEEE Trans. Ultrason. Ferroelectr. Freq. Control* **48**, 432–444 (2001).
17. C. Trillo, A. F. Doval, D. Cernadas, O. López, J. C. López, B. V. Dorrío, J. L. Fernández, and M. Pérez-Amor, "Measurement of the complex amplitude of transient surface acoustic waves using double-pulsed TV holography and a two-stage spatial Fourier transform method," *Meas. Sci. Technol.* **14**, 2127–2134 (2003).
18. C. Trillo and A. F. Doval, "Spatiotemporal Fourier transform method for the measurement of narrowband ultrasonic surface acoustic waves with TV holography," *Proc. SPIE* **6341**, 63410M (2006).
19. J. C. López-Vázquez, J. L. Deán, C. Trillo, A. F. Doval, J. L. Fernández, F. Amlani, and O. P. Bruno, "Modeling for characterizing defects in plates using two-dimensional maps of instantaneous ultrasonic out-of-plane displacement obtained by pulsed TV-holography," *Proc. SPIE* **7389**, 738937 (2009).
20. J. L. Rose, *Ultrasonic Waves in Solid Media*, pp. 200–240, Cambridge University Press, Cambridge, UK (2000).
21. J. D. Achenbach, *Reciprocity in Elastodynamics*, pp. 116–131, Cambridge University Press, Cambridge, UK (2003).
22. O. Diligent, T. Grahn, A. Bostrom, P. Cawley, and M. J. S. Lowe, "The low-frequency reflection and scattering of the S0 Lamb mode from a circular through-thickness hole in a plate: Finite Element, analytical and experimental studies," *J. Acoust. Soc. Am.* **112**, 2589–2601 (2002).
23. J. L. Deán, C. Trillo, A. F. Doval, and J. L. Fernández, "Determination of thickness and elastic constants of aluminum plates from full-field wavelength measurements of single-mode narrowband Lamb waves," *J. Acoust. Soc. Am.* **124**, 1477–1489 (2008).
24. A. F. Doval, "A systematic approach to TV-holography," *Meas. Sci. Technol.* **11**, R1–R36 (2000).
25. O. P. Bruno and S. K. Lintner, "Generalized Calderon formula and second-kind integral solvers for TE and TM problems of diffraction by open arcs" (unpublished).

J. Carlos López-Vázquez received his MPhil degree in physics from the University of Santiago de Compostela in 1988, and his PhD degree in applied physics from the University of Vigo in 1997, where is currently an associate professor. His research interests are related to optical techniques for nondestructive testing applications in industry and modeling and simulation of wave propagation phenomena.

X. Luís Deán-Ben received the diploma in automatics and electronics engineering from the Universidade de Vigo in 2004. He received the PhD degree also from the Universidade de Vigo in 2009, after completing his PhD thesis in the nondestructive testing of plates with TV holography measurements of Lamb waves.

Cristina Trillo received her automatics and electronics engineer and PhD degrees from the University of Vigo in 1999 and 2004, respectively. She joined the Department of Applied Physics of the University of Vigo in 2000 as a research associate. Her main research interests within the optical metrology group are image processing, optical measurement, and nondestructive inspection by TV holography.

Ángel F. Doval received his automatics and electronics engineer and PhD degrees from the Universities of Santiago de Compostela in 1990 and Vigo in 1997, respectively. He joined the Department of Applied Physics of the University of Vigo in 1990 as a lecturer; since 1998 he has held a senior lectureship. His research with the optical metrology group focuses on optical measurement and nondestructive inspection by digital holography, TV holography, and other interferometric techniques.

José L. Fernández received his diploma in mechanical engineering from Universidad Politécnica de Madrid in 1984, and his PhD degree in engineering in 1988 from Universidad de Santiago de Compostela. He is currently a full professor of applied physics and head of the optical metrology group in the University of Vigo. His research interest includes dimensional measurements and nondestructive inspection by optical techniques, in particular TV holography, interferometry, and moiré techniques.

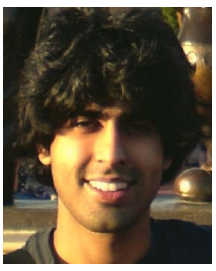

Faisal Amlani is a PhD student in the Department of Applied and Computational Mathematics at the California Institute of Technology (Caltech) in Pasadena, California.

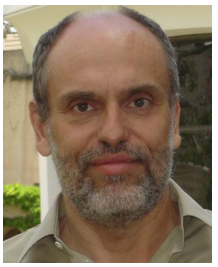

Oscar P. Bruno received his PhD degree from the Courant Institute of Mathematical Sciences, New York University. Following graduation, he held a position for two years as a visiting assistant professor with the University of Minnesota, and then joined the faculty of the Georgia Institute of Technology (Georgia Tech), where he held positions as an assistant professor and associate professor. After a four-year period with Georgia Tech, he joined the faculty of the California Institute of Technology (Caltech), Pasadena, where he is now a professor in the Department of Applied and Computational Mathematics, having served as executive officer during 1998 to 2000. His research interests lie in areas of optics, elasticity and electromagnetism, remote sensing and radar, overall electromagnetic and elastic behavior of materials (solid, fluids, composites materials, and multiple-scale geometries), and phase transitions. He is a recipient of a Friedrichs Award for an outstanding dissertation in mathematics from the Courant Institute, a Young Investigator Award from the National Science Foundation, and a Sloan Foundation Fellowship.